

Catalytic Assembly of the Mitotic Checkpoint Inhibitor BubR1-Cdc20 by a Mad2-Induced Functional Switch in Cdc20

Joo Seok Han,^{1,2} Andrew J. Holland,^{1,2,5} Daniele Fachinetti,^{1,2} Anita Kulukian,^{1,3,4} Bulent Cetin,^{1,2} and Don W. Cleveland^{1,2,*}

¹Ludwig Institute for Cancer Research

²Department of Cellular and Molecular Medicine

³Department of Biology

University of California at San Diego, La Jolla, CA 92093, USA

⁴Laboratory of Mammalian Cell Biology and Development, The Rockefeller University, New York, NY 10065, USA

⁵Present address: Department of Molecular Biology & Genetics, Johns Hopkins University School of Medicine, Baltimore, MD 21205, USA

*Correspondence: dcleveland@ucsd.edu

<http://dx.doi.org/10.1016/j.molcel.2013.05.019>

SUMMARY

The mitotic checkpoint acts to maintain chromosome content by generation of a diffusible anaphase inhibitor. Unattached kinetochores catalyze a conformational shift in Mad2, converting an inactive open form into a closed form that can capture Cdc20, the mitotic activator of the APC/C ubiquitin ligase. Mad2 binding is now shown to promote a functional switch in Cdc20, exposing a previously inaccessible site for binding to BubR1's conserved Mad3 homology domain. BubR1, but not Mad2, binding to APC/C^{Cdc20} is demonstrated to inhibit ubiquitination of cyclin B. Closed Mad2 is further shown to catalytically amplify production of BubR1-Cdc20 without necessarily being part of the complex. Thus, the mitotic checkpoint is produced by a cascade of two catalytic steps: an initial step acting at unattached kinetochores to produce a diffusible Mad2-Cdc20 intermediate and a diffusible step in which that intermediate amplifies production of BubR1-Cdc20, the inhibitor of cyclin B ubiquitination, by APC/C^{Cdc20}.

INTRODUCTION

The mitotic checkpoint (also known as the spindle assembly checkpoint) delays the irreversible transition into anaphase until kinetochores on all chromosomes successfully attach to spindle microtubules. Each unattached kinetochore produces an inhibitory signal(s) that blocks ubiquitination of cyclin B and securin by inhibiting Cdc20, the preanaphase activator of the E3 ubiquitin ligase, the anaphase-promoting complex or cyclosome (APC/C) (reviewed in [Lara-Gonzalez et al., 2012](#); [Peters, 2006](#)). Anaphase onset is triggered by silencing the checkpoint-derived inhibitor and the subsequent degradation of cyclin B and securin. Critical components of the mitotic checkpoint include Bub1, Bub3, Mad1, Mad2, Mad3 (known as BubR1 outside of

yeast), and Mps1 ([Hoyt et al., 1991](#); [Li and Murray, 1991](#); [Weiss and Winey, 1996](#)).

Mad2 is an essential mitotic checkpoint protein that has been shown to directly bind to Cdc20 ([Fang et al., 1998](#)). Structural studies have revealed that Mad2 undergoes a major conformational change (from an open form to a closed form) when it binds to Cdc20 or Mad1 ([Luo et al., 2000, 2002, 2004](#); [Mapelli et al., 2007](#); [Sironi et al., 2001, 2002](#)). In vivo and in vitro fluorescence recovery after photobleaching has led to a model in which open Mad2 is converted to a closed form by recruitment to a stably bound Mad1/Mad2 complex at each unattached kinetochore ([Shah et al., 2004](#); [Vink et al., 2006](#)). This second molecule of Mad2 then quickly cycles on and off unattached kinetochores ([De Antoni et al., 2005](#); [Mapelli et al., 2006](#); [Nezi et al., 2006](#); [Shah et al., 2004](#); [Vink et al., 2006](#)). In vitro reconstitution has established that unattached kinetochores with stably bound Mad1 serve as Mad2 templates to catalyze the production of a diffusible Cdc20 inhibitor ([Kulukian et al., 2009](#)).

BubR1 has also been shown to associate with Cdc20 ([Wu et al., 2000](#)) and can inhibit Cdc20 activation of APC/C either alone ([Tang et al., 2001](#)) or in combination with Mad2 ([Fang, 2002](#); [Kulukian et al., 2009](#); [Lara-Gonzalez et al., 2011](#)). Two Cdc20 binding domains have been identified in BubR1: one within the N-terminal Mad3 homology domain and a second at an internal site ([Davenport et al., 2006](#)). Mad2 can enhance BubR1 association with Cdc20 ([Davenport et al., 2006](#); [Kulukian et al., 2009](#)), but the mechanistic contribution(s) to mitotic checkpoint signaling of the two Cdc20 binding domains in BubR1 remains to be established.

Attempts have been made to identify the mitotic checkpoint inhibitor produced by unattached kinetochores ([Chao et al., 2012](#); [Kulukian et al., 2009](#); [Nilsson et al., 2008](#); [Sudakin et al., 2001](#)). While BubR1, Bub3, and Mad2 have all been found to be complexed with Cdc20 during mitotic checkpoint-mediated arrest, there are major discrepancies in the reported level of Mad2 in the inhibitory complex, spanning from equimolar ([Chao et al., 2012](#); [Sudakin et al., 2001](#)) to negligible ([Nilsson et al., 2008](#)) levels compared to Cdc20. Correspondingly, multiple models have been put forward for how APC/C^{Cdc20} is inhibited. One proposal, based on recent evidence in budding

yeast, is that the function of Mad3 (i.e., BubR1) is to promote the inhibition of Cdc20 by Mad2 (Lau and Murray, 2012). An alternative model for Cdc20 inhibition relies on cooperative binding of Mad2 and Mad3. Evidence for this model comes from a crystal structure of a fission yeast mutant of Mad2 locked in the closed conformation and complexed with portions of Mad3 and Cdc20. Consistent with this latter model, activity of APC/C^{Cdc20} has been proposed to be influenced by the sequestration of Cdc20's N-terminal APC/C recognition motifs by Mad2 (Chao et al., 2012; Izawa and Pines, 2012). Lastly, Mad3/BubR1 may act as a pseudosubstrate inhibitor that competes with substrates for Cdc20 binding in a KEN-box-dependent manner (Burton and Solomon, 2007).

In all of the proposed models, it remains unclear how a single unattached kinetochore can act to generate global inhibition of APC/C^{Cdc20} activity. Using a combination of purified components and cultured cells, we now identify two sequential, interlocking catalytic steps in the production of the mitotic checkpoint inhibitor in which BubR1, not Mad2, blocks the activity of APC/C^{Cdc20}. In an initial catalytic step, the Mad1/Mad2 complex acts locally at unattached kinetochores to catalyze the production of closed Mad2 bound to Cdc20. Subsequently, closed Mad2 then functions catalytically as a diffusible loader for generating BubR1 binding to a previously inaccessible site in Cdc20. This produces Cdc20 bound to BubR1 as the functional mitotic checkpoint-derived inhibitor that selectively blocks ubiquitination of cyclin B and securin by APC/C^{Cdc20}.

RESULTS

Inhibition of APC/C^{Cdc20} by Mad2 and the Conserved Mad3 Cdc20 Binding Site of BubR1 Is Essential for the Mitotic Checkpoint

To determine the contribution to mitotic checkpoint signaling of the Cdc20 binding sites in BubR1, endogenous BubR1 was replaced by a similar level (Figures 1A and 1B and Figures S1A–S1C available online) of MycGFP-BubR1 variants containing either or both Cdc20 binding domains. As expected, suppression of endogenous BubR1 resulted in premature mitotic exit from an unperturbed mitosis, which was rescued by expression of full-length BubR1 (BubR1_{1–1050}) or a variant (BubR1_{1–363}) that included the N-terminal, Mad3 homology domain Cdc20 binding site but bound neither Bub3 nor kinetochores (Figures 1C and S1D). Similarly, both full-length (BubR1_{1–1050}) and BubR1 variants with the N-terminal Cdc20 binding site (BubR1_{1–363} or BubR1_{1–477}) sustained long-term nocodazole-induced mitotic arrest, whereas BubR1-depleted cells exited mitosis within 35 min (Figure 1D).

The BubR1 N-terminal-mediated mitotic checkpoint arrest was dependent on Mad2, as it was completely eliminated by small interfering RNA (siRNA)-mediated reduction in Mad2 (Figure 1E). In contrast, replacement of endogenous BubR1 with variants deleted in the Cdc20 binding site within the Mad3 homology domain was unable to mediate checkpoint signaling in both unperturbed mitosis (Figures 1C and S1D) and nocodazole-treated cells (Figure 1D). This effect did not depend on whether the BubR1 fragments contained (BubR1_{357–1050}) or lacked (BubR1_{357–700}) the BubR1 kinase domain. Full-length

BubR1 mediated nocodazole-induced mitotic arrest longer than BubR1 variants with only the N-terminal Cdc20 binding site, consistent with a possible role of the internal Cdc20 binding site in maintaining chronic mitotic checkpoint signaling.

To determine how BubR1 generated a mitotic checkpoint inhibitor together with Mad2, full-length recombinant BubR1 and BubR1 fragments containing either Cdc20 binding domain were expressed, purified (Figures 1F and S1E), and incubated with Cdc20 along with Bub3 in the presence or absence of Mad2. Inactive APC/C was added and incubated, and the APC/C was subsequently recovered (with an antibody to Cdc27). Finally, cyclin B was added along with E1, the E2 UbcH10, and ubiquitin. APC/C^{Cdc20} ubiquitination activity was then measured by the increase of multiubiquitinated cyclin B or by the reduction of unubiquitinated cyclin B (Figures S1F and S1G). While full-length wild-type Mad2 alone produced no inhibition of Cdc20's ability to activate APC/C (Figure S1G), addition of Bub3 and full-length BubR1 (hereafter BubR1^{FL}) along with Cdc20 significantly reduced subsequent APC/C-mediated cyclin B ubiquitination in a dose-dependent manner (Figures S1G, top: lanes 3–6, and S1H, red triangles).

Synergistic inhibition of Cdc20 activation of APC/C was produced by coaddition of BubR1^{FL}-Bub3 and Mad2 (Figures S1G, top: lanes 11–14, and S1H, blue squares). Assay of Bub3 and a BubR1 variant containing only BubR1's internal Cdc20 binding site (BubR1_{357–1050}, to be referred to hereafter as BubR1^C) produced a level of inhibition of cyclin B ubiquitination similar to that of a comparable amount of Bub3-BubR1^{FL}; however, in the absence of the Mad3-homology region Cdc20 binding site, inhibition was not enhanced by coincubation with Mad2 (Figures S1G, bottom, and S1J). By contrast, BubR1_{1–477} (carrying the Mad3 homology region Cdc20 binding domain and to be referred to hereafter as BubR1^N) had no APC/C^{Cdc20} inhibitory activity when complexed with Bub3 (Figures S1G, middle: lanes 3–6, and S1I, red triangles), but inhibition was strongly enhanced by addition of an equivalent amount of Mad2 (Figures S1G, middle: lanes 11–14 and 1I, blue squares), which again had no inhibitory activity by itself. Moreover, BubR1^N-Bub3 almost completely inhibited already active APC/C^{Cdc20} when Mad2 was present (Figure 1G). In contrast, BubR1^C-Bub3 produced minimal APC/C^{Cdc20} inhibition regardless of the presence of Mad2 (Figures 1G and 1H). Thus, the N-terminal, but not the internal, Cdc20 binding domain of BubR1 can mediate Mad2-dependent inhibition of APC/C^{Cdc20}, reproducing the in vivo situation (Figures 1C and 1D).

A Conformational Change in Mad2 Is Rate Limiting for Inhibition of APC/C^{Cdc20} by Mad2 and BubR1^N

To determine how Mad2 facilitated BubR1^N-dependent inhibition of APC/C^{Cdc20}, we compared inhibition produced by wild-type Mad2, which exists in an open conformation that only slowly and spontaneously converts to a closed form (Yang et al., 2008), with two Mad2 mutants: closed Mad2 (Mad2^{L13A}) (Yang et al., 2007) and open Mad2 (Mad2^{ΔC}) (Luo et al., 2000) (Figure S2A). While closed Mad2^{L13A} alone (Figures S2D and S2E) had no APC/C inhibitory activity when used at equal stoichiometry with Cdc20, it was much more potent than wild-type Mad2 in promoting BubR1^N-mediated APC/C inhibition, producing comparable inhibition at concentrations five times lower than needed

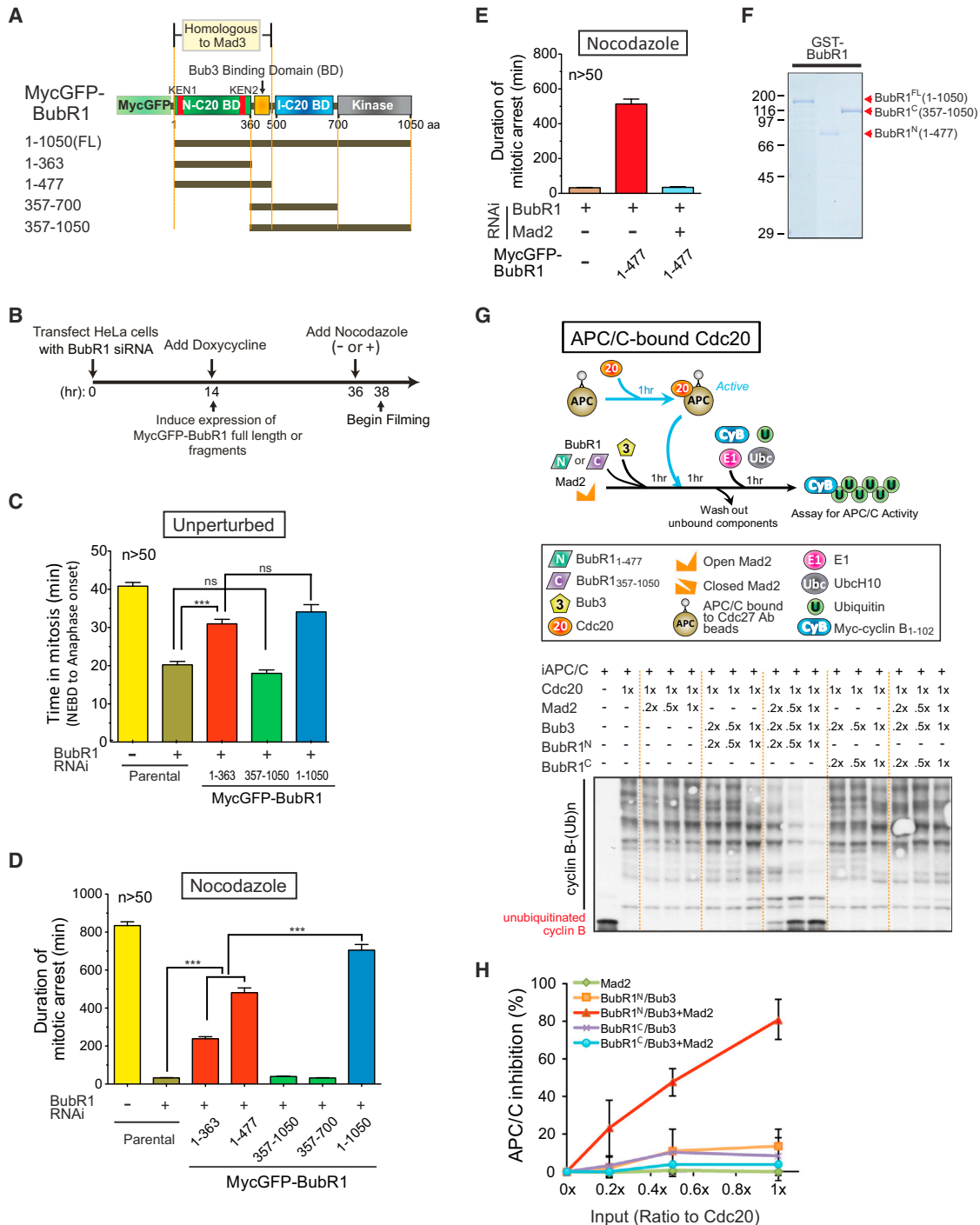


Figure 1. Inhibition of APC/C^{Cdc20} by Mad2 and BubR1^N Is Critical for the Mitotic Checkpoint

(A) Schematic of the MycGFP-BubR1 transgenes stably expressed in HeLa cells, with functional domains of BubR1 highlighted. (B) Schematic of the protocol used for replacement of endogenous BubR1 with various BubR1 transgenes. (C and D) Time-lapse microscopy was used to determine mitotic timing in (C) an unperturbed mitosis and (D) in the presence of nocodazole (100 ng/ml). (E) Time-lapse microscopy was used to determine mitotic timing in nocodazole after replacing endogenous BubR1 with MycGFP-BubR1^N. Mad2 was codepleted where indicated using siRNA. Bars in (C–E) represent the mean of at least 50 cells from two independent experiments. Error bars represent SEM. ***p < 0.0001. (F) Purified recombinant BubR1 fragments, assessed by Coomassie blue staining. (G and H) In vitro generation of an inhibitor of preactivated APC/C^{Cdc20} for ubiquitination of cyclin B₁₋₁₀₂ (G). Inhibitory activity was measured in (H) by depletion of unubiquitinated cyclin B₁₋₁₀₂. Data represent mean ± SEM. See also Figure S1.

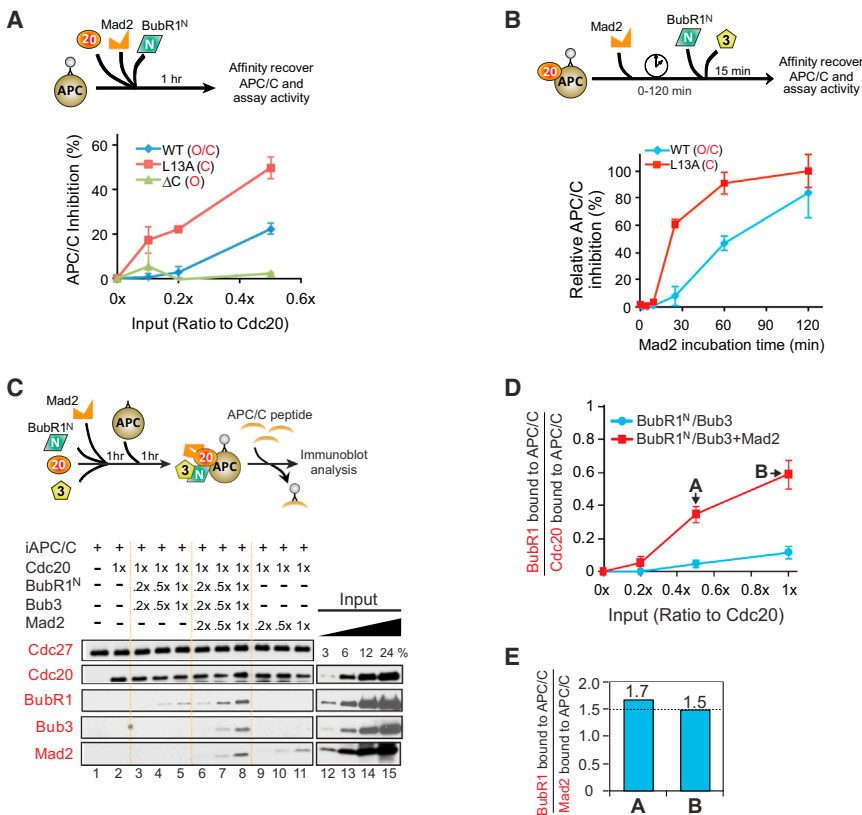


Figure 2. A Conformational Change in Mad2 Facilitates BubR1^N's Ability to Inhibit Cdc20-Mediated Activation of APC/C

(A) Top: increasing amounts of BubR1^N, and Mad2 (L13A, WT, and ΔC) were incubated with Cdc20 and APC/C. APC/C was affinity purified and assayed for activity. Bottom: plot of percent of APC/C inhibition. Error bars represent SEM (n = 3). (B) Testing how Mad2 conformation affects inhibition of preactivated APC/C^{Cdc20} by BubR1^N and wild-type Mad2 or a Mad2 variant locked in the closed conformation (Mad2^{L13A}). Data represent mean ± SEM (n = 3). (C) Top: schematic for complexes bound to APC/C^{Cdc20}. Bottom: Mad2 dependence for BubR1^N binding to APC/C^{Cdc20}. (D) The molar ratio of BubR1^N bound to APC/C compared with Cdc20 bound to APC/C from lanes 3–8 in (C) was measured against a dilution series of purified proteins. Plot displays the mean from two independent assays. Error bars represent SEM. (E) Stoichiometry of BubR1 and Mad2 assembled into Cdc20 complexes (at the added stoichiometries denoted by A and B in D). See also Figure S2.

for wild-type Mad2 (Figures 2A and S2B). In contrast, BubR1^N produced no inhibition of APC/C in the presence of open Mad2^{ΔC} (Figures 2A and S2B).

In light of our evidence for catalytic production of a Mad2-Cdc20 inhibitor in the presence of unattached kinetochores containing the Mad1/Mad2 complex (Kulukian et al., 2009), we tested if addition of closed Mad2—the proposed product of immobilized Mad1-Mad2 at kinetochores (De Antoni et al., 2005; Kulukian et al., 2009; Luo et al., 2002)—accelerated Mad2-dependent BubR1^N inhibition of APC/C^{Cdc20}. In the absence of BubR1^N-Bub3, even a stoichiometric level (relative to Cdc20) of closed Mad2^{L13A} did not mediate any inhibition of cyclin B ubiquitination by APC/C^{Cdc20} (Figures S2D and S2E). Closed Mad2 (Mad2^{L13A}) was much more potent than wild-type Mad2 in promoting BubR1^N-mediated APC/C inhibition, producing an initial rate of inhibition eight times faster than wild-type Mad2 and yielding much higher inhibition at early times (e.g., at 25 min there was ~60% inhibition from Mad2^{L13A} versus only 8% inhibition with Mad2^{WT}) (Figures 2B and S2C). Thus, the rate of formation of the APC/C^{Cdc20} inhibitor by BubR1^N-Bub3 depended on the concentration of closed Mad2, consistent with the idea of kinetochore-catalyzed conformational change in Mad2 as an initiating step in mitotic checkpoint signaling.

The Mad2-Dependent Complex of BubR1^N-APC/C^{Cdc20} Contains Substoichiometric Mad2

To identify the mechanism by which Mad2 stimulated BubR1-dependent inhibition of APC/C^{Cdc20}, we affinity purified APC/C

after incubation with BubR1^N, Bub3, Mad2, and Cdc20. In the absence of Mad2, only a trace level of BubR1^N-Bub3 associated with APC/C^{Cdc20}. This association was increased ~6-fold by coincubation with Mad2 (yielding 0.6 molecules of BubR1 bound per molecule of Cdc20) (Figures 2C and 2D). Under the same conditions, cyclin B ubiquitination by APC/C^{Cdc20} was reduced by a comparable percentage (Figure 1H), consistent with inhibition of APC/C^{Cdc20} activity by stoichiometric binding of BubR1^N. Although Mad2 facilitated BubR1^N association with APC/C^{Cdc20}, the level of Mad2 bound to the produced APC/C^{Cdc20} complex was lower than that of BubR1^N (Figure 2E).

Mad2 Enables BubR1 Binding to APC/C^{Cdc20} without Necessarily Remaining Bound

While a consensus has emerged that the initiating event in mitotic checkpoint signaling is production of Mad2-Cdc20 by unattached kinetochores, widely divergent levels of Mad2 have been reported (Kulukian et al., 2009; Nilsson et al., 2008; Sudakin et al., 2001; Westhorpe et al., 2011) or predicted (Chao et al., 2012) in the mitotic checkpoint complexes, leaving the molecular identity of the checkpoint-produced inhibitor of APC/C^{Cdc20} a central unresolved question. Moreover, although Mad2-stimulated BubR1^N-Cdc20 binding was increased at higher Mad2 levels (Figure S2F), the level of Mad2 bound to APC/C^{Cdc20} in the final complex was lower than the level of BubR1^N (Figure 2E). Consistent with this, immunopurified Cdc20 molecules from nocodazole-arrested mitotic cells were associated with 3-fold more BubR1 than Mad2 (Figures S2G and S2H), suggesting dissociation of Mad2 from Cdc20 after enabling initial binding of BubR1^N to Cdc20.

To determine if continued Mad2-Cdc20 association is required for maintaining a BubR1 association with APC/C^{Cdc20},

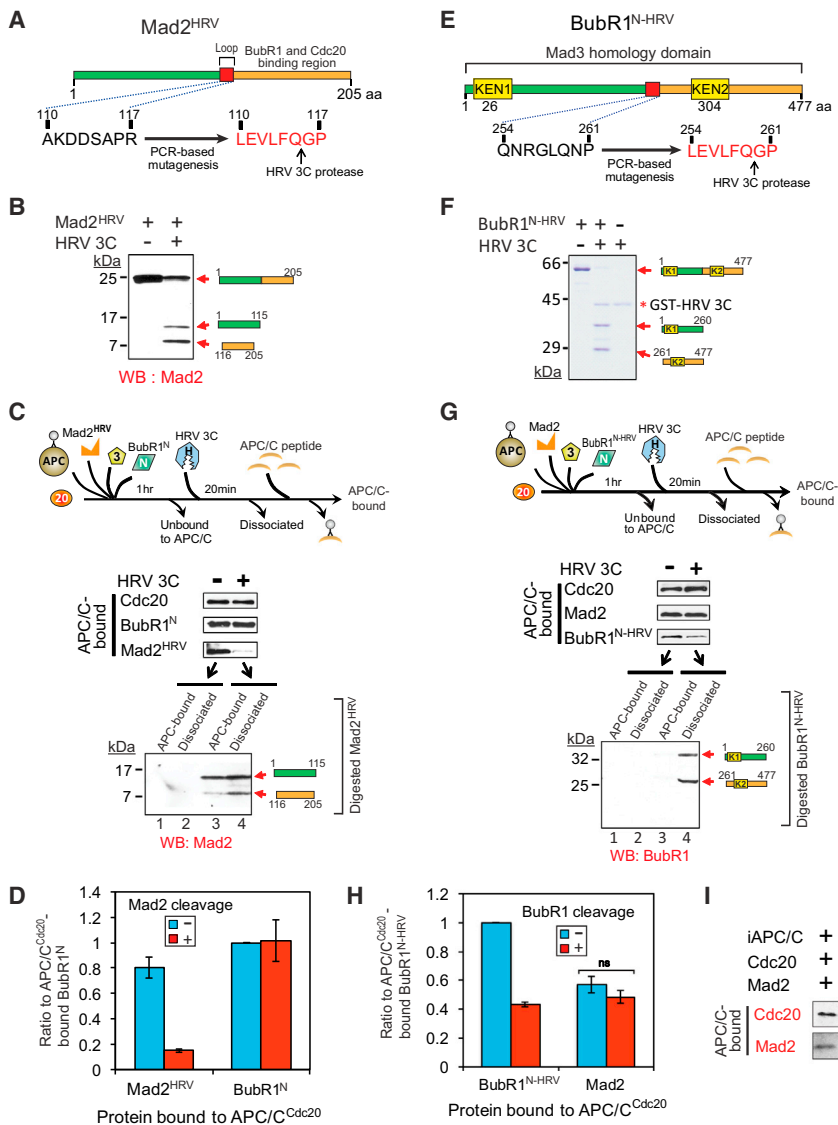


Figure 3. Maintaining the Association of BubR1^N with Cdc20 Does Not Require the Mad2-Cdc20 Interaction

(A) Schematic of a Mad2 variant modified to contain an HRV 3C cleavage site. (B) Immunoblot showing HRV 3C-mediated cleavage of Mad2^{HRV} in vitro. Mad2^{HRV} was incubated at room temperature for 20 min in the presence or absence of HRV 3C protease. (C) After incubation with BubR1^N, Bub3, Mad2^{HRV}, and Cdc20, APC/C was affinity purified to remove unbound components. Following incubation with or without HRV 3C protease, dissociated components were washed away, and APC/C was peptide eluted from beads and analyzed for associated components by immunoblotting. The supernatant from the protease digestion mixture was collected and analyzed for release of the digested Mad2^{HRV} fragments. (D) The amount of APC/C-bound BubR1^N or Mad2^{HRV} in (C) was measured. Values are plotted as the molar ratio of APC/C-bound Mad2^{HRV} compared with APC/C-bound BubR1^N. The level of APC/C-bound BubR1^N without protease treatment was set to 1. Bars represent the mean. Error bars represent SEM (n = 3). (E) Schematic of an HRV 3C-cleavable variant of BubR1^N. (F) HRV 3C-mediated digestion of the cleavable BubR1^N in vitro. Cleavable BubR1^N was incubated at room temperature for 20 min in the presence or absence of HRV 3C prior to analysis. (G and H) Effect of forced BubR1^N release on the association of Mad2 with APC/C^{Cdc20}. (G) Experimental procedure is the same as in (C). (H) Values were plotted as the molar ratio compared with APC/C-bound BubR1^{N-HRV}. The level of APC/C-bound cleavable BubR1^N without the protease treatment was set to 1. Bars represent the mean. Error bars represent SEM (n = 3). ***p < 0.0001. (I) Assay of Mad2 binding to APC/C in the presence and absence of Cdc20. See also Figure S3.

we created a Mad2 mutant (hereafter Mad2^{HRV}) that can be removed from an initial APC/C^{Cdc20} complex through cleavage by the sequence-specific HRV 3C (human rhinovirus 3C) protease (Cordingley et al., 1990) (Figure 3A). Upon incubation with HRV 3C protease, the 24 kDa Mad2^{HRV} was cleaved into 15 kDa and 9 kDa fragments (Figure 3B). The digested Mad2^{HRV} fragments were nonfunctional as inhibitors of APC/C^{Cdc20} (Figure S3). APC/C was incubated with Cdc20, BubR1^N, and Bub3 (at 1:1:1 stoichiometries) and a 5-fold excess of Mad2^{HRV}, a concentration that produces similar levels of BubR1^N and Mad2 bound to Cdc20 (Figure 3D). Protease treatment reduced Mad2^{HRV} bound to APC/C^{Cdc20} by 80% (Figures 3C and 3D), with most of the C-terminal Mad2^{HRV} fragment (containing residues required for binding to Cdc20 and Mad3, the yeast homolog of BubR1; Chao et al., 2012) dissociated from APC/C^{Cdc20} (Figure 3C, lanes 3 and 4). Importantly, the level of BubR1^N bound to Cdc20 remained almost unchanged, despite

a >5-fold reduction of Cdc20-bound Mad2 (Figures 3C and 3D). Taken together, these findings demonstrate that Mad2 stimulates the initial BubR1^N-Cdc20 interaction but is dispensable for maintaining this association.

BubR1, Not Mad2, Binds to Cdc20 in the Final APC/C^{Cdc20} Inhibitor

To test if BubR1^N is a bona fide APC/C^{Cdc20} inhibitor, we created a BubR1 mutant (hereafter BubR1^{N-HRV}) that contains the recognition sequence for HRV 3C protease between amino acids 254–261. Incubation of purified BubR1^{N-HRV} with protease produced 34 kDa and 26 kDa fragments, respectively (Figure 3F). Bead-immobilized APC/C was again incubated with Cdc20, BubR1^{N-HRV}, and Bub3 (at 1:1:1 stoichiometries) and a 5-fold excess of Mad2. A total of 60% of APC/C BubR1^{N-HRV} was cleaved by protease addition, with all of the cleavage products released from the APC/C complexes (Figure 3G); however, this

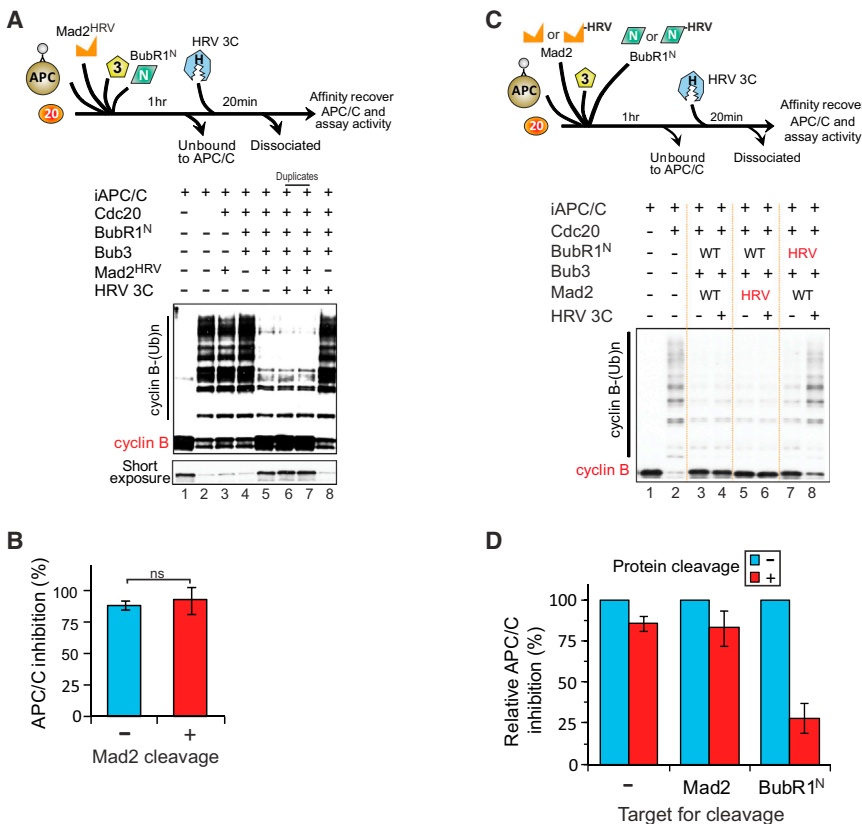


Figure 4. The Mad3 Homology Domain of BubR1, but Not Mad2, Is the Effector for APC/C^{Cdc20} Inhibition In Vitro

(A and B) Testing if Mad2 binding to Cdc20 is required for APC/C^{Cdc20} inhibition. (A) Bead-bound APC/C was incubated with combinations of BubR1^N, Bub3, Mad2^{HRV}, and Cdc20 followed by removal of components unbound to APC/C. Buffer either containing HRV 3C protease or not was added for 20 min prior to APC/C activity assay. (B) Graph quantifying percent inhibition of APC/C with or without protease incubation in (A). Bars represent the mean \pm SEM (n = 3). ns, not significant. (C) Assay to determine whether BubR1^N or Mad2 is an effector for APC/C^{Cdc20} inhibition after HRV 3C protease-mediated digestion and dissociation of BubR1^{N-HRV} or Mad2^{HRV} from inhibited APC/C^{Cdc20}. (D) Quantification of inhibition of APC/C activity in (C). Bars represent mean \pm SEM (n = 3). See also Figure S4.

(D) Bars represent mean \pm SEM (n = 3). See also Figure S4.

did not affect the amount of Mad2 retained (Figures 3G and 3H). Additionally, since Mad2 association with APC/C was completely dependent on the presence of Cdc20 (Figure 3I), the Mad2 remaining in the BubR1-depleted complexes must be bound to Cdc20, and the Mad2-Cdc20 interaction does not depend on the BubR1-Cdc20 interaction.

To address the individual function of Mad2 and BubR1^N in inhibiting activity of APC/C^{Cdc20}, the inhibitor-bound APC/C complex containing BubR1^{N-HRV} or Mad2^{HRV} was incubated with the HRV 3C protease. Nearly quantitative digestion of Mad2 did not significantly alter APC/C inhibition (Figures 4A–4D). Digestion of BubR1^{N-HRV}, on the other hand, reduced APC/C inhibition by 70% (Figures 4C, lanes 7 and 8, and 4D, right set), with the residual 30% inhibition of APC/C attributable to the incomplete digestion of the BubR1^{N-HRV} (Figures 3F and 3G). Similarly, digestion of BubR1^{FL-HRV} (full-length BubR1 that contains the recognition sequence for HRV 3C protease) bound to APC/C^{Cdc20} significantly reduced APC/C inhibition (Figure S4). Taken together, our results demonstrate that in vitro BubR1, but not Mad2, is the effective inhibitor of APC/C^{Cdc20} and, in complexes containing both BubR1 and Mad2, it is Cdc20 binding to BubR1 that inhibits recognition of cyclin B by APC/C^{Cdc20}.

BubR1, Not Mad2, Is the Mitotic Checkpoint Inhibitor In Vivo

To test the in vivo requirement of BubR1 and Mad2 for inhibition of APC/C^{Cdc20}, we took advantage of a recently described auxin-inducible degron (AID) system (Holland et al., 2012; Nishi-

mura et al., 2009). We established stable cell lines expressing doxycycline-inducible and RNAi-resistant GFP-AID-tagged BubR1 or Mad2-AID-YFP (Figure 5A). Addition of the auxin derivative IAA to cells arrested in mitosis induced rapid destruction of both AID-tagged BubR1 and Mad2 with time for 50% degradation (t_{1/2}) of 15 and 30 min, respectively, while proteins associated with either remained stable (Figures 5B and S5A). Suppression of endogenous BubR1 or Mad2 by transfection of appropriate siRNAs and doxycycline induction led to their replacement with GFP-AID-BubR1 or Mad2-AID-YFP (Figure 5D).

Cdc20 has been shown to undergo autoubiquitination and turnover during mitosis (King et al., 2007; Nilsson et al., 2008; Pan and Chen, 2004; Reddy et al., 2007; Varetta et al., 2011), leading to disassembly of the Cdc20-associated checkpoint inhibitor(s). Since the rapid turnover of checkpoint inhibitor(s) in vivo would preclude identifying whether Mad2 or BubR1 is the final inhibitor(s) of APC/C^{Cdc20}, we codepleted p31^{comet} to stabilize Cdc20 inhibitor(s) (Jia et al., 2011; Mapelli et al., 2006; Reddy et al., 2007; Teichner et al., 2011; Varetta et al., 2011; Westhorpe et al., 2011). Following checkpoint activation and IAA-induced degradation of Mad2-AID-YFP or GFP-AID-BubR1, the duration of mitotic checkpoint-mediated arrest was determined by time-lapse microscopy. Addition of IAA to mitotically arrested Mad2-AID-YFP-expressing cells induced destruction of 90% of Mad2-AID-YFP within 60 min, but, remarkably, all cells remained arrested in mitosis (Figure 5E, red). Indeed, after Mad2-AID-YFP degradation, 60% of cells sustained a mitotic arrest for >6 hr, similar to the duration observed in cells not treated with IAA and in which Mad2-AID-YFP remained stable (Figure 5E, green). Mad2 was essential for initiating this sustained arrest, however, as destruction of Mad2-AID-YFP prior to mitotic entry (in the presence of nocodazole)

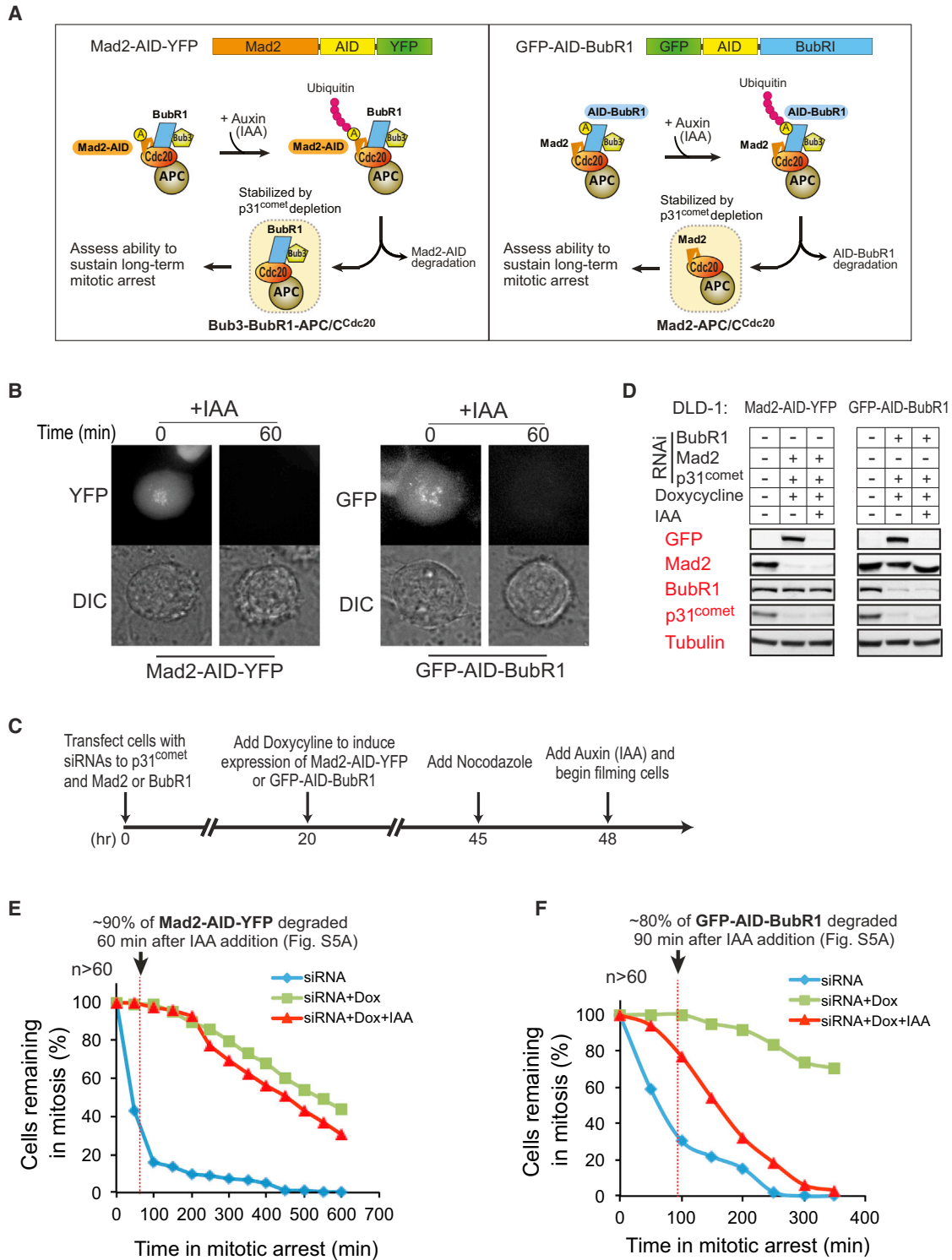


Figure 5. BubR1, Not Mad2, Is Required to Sustain Inhibition of APC/C^{Cdc20} In Vivo

(A) Schematic for the inducible destruction of Mad2-AID-YFP or GFP-AID-BubR1 in mitotic cells using an auxin-inducible protein degradation system.

(B) Microscopic images showing auxin (indoleacetic acid, IAA)-induced mitotic degradation of Mad2-AID-YFP (left) or GFP-AID-BubR1 (right).

(C) Schematic of the protocol used to deplete endogenous p31^{comet} and replace Mad2 or BubR1 with an AID-tagged version. Degradation of AID-tagged proteins was induced with IAA (500 μ M) and cells monitored by time-lapse microscopy.

(D) Immunoblot showing the levels of various proteins before and after IAA-induced degradation of (left) Mad2-AID-YFP or (right) GFP-AID-BubR1.

(legend continued on next page)

lead to rapid mitotic exit (Figures S5B and S5C). By contrast, IAA-induced destruction of GFP-AID-BubR1 not only disrupted the extended mitotic arrest, but provoked mitotic exit before BubR1 was completely degraded (Figure 5F, red). Taken together, as was seen in our *in vitro* observations (Figure 4), these efforts demonstrate that under conditions in which disassembly of mitotic checkpoint complexes is dampened (by depletion of p31^{comet}), BubR1, not Mad2, is required to sustain inhibition of APC/C^{Cdc20}.

Mad2 Acts Catalytically to Produce an APC/C^{Cdc20} Inhibitor Containing BubR1, but Not Itself

We next tested if a single molecule of Mad2 is capable of facilitating the production of multiple BubR1-APC/C^{Cdc20} complexes. As expected, at stoichiometric levels of Mad2, BubR1^N-mediated inhibition of APC/C^{Cdc20} increased in a time-dependent manner, reaching 100% inhibition within 2 hr (Figures 6A and 6B). At concentrations of Mad2 10-fold below that of Cdc20 or BubR1, APC/C^{Cdc20} inhibition also increased over time, but at a slower rate and with biphasic kinetics, reaching ~70% inhibition by 4 hr. The initial rate of APC/C^{Cdc20} inhibition was slow (5.5% inhibition of APC/C^{Cdc20} per hr), but the rate of inhibitor formation in the presence of a substoichiometric level of Mad2 accelerated (by 3.6-fold) by the end of 1 hr (to 20% inhibition of APC/C^{Cdc20} per hr). In contrast, addition of a substoichiometric level of BubR1^N-Bub3 mediated inhibition of APC/C^{Cdc20} activity only in proportion to the level of added BubR1, indicating that the inhibition was limited by the available BubR1 (Figure 6B, light blue line).

We further tested (in an *in vivo* context) (schematic in Figure 6C) this model in which Mad2 and BubR1 play discrete roles as a catalytic loader and an effector for Cdc20 inhibition, respectively, with the accelerating rate of APC/C^{Cdc20} inhibition *in vitro* reflecting Mad2 dissociation from Cdc20 in a conformation that can rebind another molecule of Cdc20. To do this, cells were first depleted by ~90% for either BubR1 or Mad2 using siRNAs (Figure 6D). To stabilize accumulated Cdc20 inhibitor(s), transfection of siRNA was used to codeplete p31^{comet}. Nocodazole was added to sustain activation of the mitotic checkpoint, and a 26S proteasome inhibitor was added to inhibit cyclin B destruction, thereby allowing the accumulation of mitotic checkpoint inhibitor(s). After 2 hr, the proteasome inhibitor was removed, and the duration of remaining mitotic arrest was determined by time-lapse microscopy.

In cells with normal levels of Mad2, but with ~10% of the normal BubR1 level, washout of the proteasome inhibitor yielded mitotic exit, with >60% of cells exiting mitosis within 4 hr (Figure 6E, blue solid line). By contrast, cells in which Mad2 levels were reduced to ~10% of the normal level sustained a mitotic arrest for 16 hr after washout of the proteasome inhibitor (Figure 6E, red solid line). The normal cellular stoichiometries of BubR1 and Cdc20 have been determined to be 1:1, with Mad2 between 1.3- (Tang et al., 2001) and 3-fold (Nilsson et al.,

2008) higher. Thus, a 90% depletion of Mad2 reduces it to a level between 13% and 30% of that of Cdc20. Nevertheless, our evidence demonstrates that this limited level of Mad2 can sustain long-term checkpoint signaling if a sufficient time window is provided to allow a BubR1-containing mitotic checkpoint inhibitor to accumulate, consistent with a model in which Mad2 acts catalytically to load BubR1 onto Cdc20.

Mad2 Binding Induces a Functional Switch in Cdc20, Enabling BubR1 Binding

Our finding that APC/C-bound Cdc20 association with BubR1^N is significantly enhanced by its prior binding to Mad2 (Figures 2D and S2F), along with a previous yeast two-hybrid study (Davenport et al., 2006), suggested a model in which the BubR1 binding site within the C-terminal WD40 repeats of Cdc20 may be initially inaccessible as the result of self-association of the Cdc20 amino- and carboxy-terminal domains. To test this directly, we expressed and purified Cdc20₁₋₁₆₃ (hereafter called Cdc20^N) and GST-Cdc20₁₆₆₋₄₉₉ (to be referred to as GST-Cdc20^C) (Figures 7A and 7B). After mixing Cdc20^N and Cdc20^C, followed by purification by glutathione affinity, GST-Cdc20^C, but not GST, copurified Cdc20^N (Figure 7C), demonstrating a direct association between the two domains. Moreover, preincubation of Cdc20^N with Cdc20^C reduced subsequent Cdc20^C association with BubR1^N (Figure 7D), consistent with blocking BubR1 binding through an intramolecular interaction between two domains in Cdc20^{FL}.

Further, addition of wild-type Mad2, but not the Cdc20-binding defective Mad2^{ΔC}, to GST-Cdc20^N and Cdc20^C reduced association of the two Cdc20 domains (Figure 7E). Most importantly, while BubR1^N did not bind to Cdc20^{FL}, Mad2 addition enabled this interaction, producing BubR1^N-Cdc20^{FL}-Mad2 complexes (Figure 7F). By contrast, BubR1^N bound Cdc20^C directly, and this interaction was unaffected by Mad2 addition. Thus, initial Mad2 binding to the N terminus of Cdc20^{FL} relieved the inhibition of Cdc20 from its binding to BubR1^N, with only a substoichiometric amount of Mad2 remaining in the final Cdc20^{FL}-BubR1^N-Bub3 complex.

DISCUSSION

The initiating feature of the checkpoint signaling pathway is a catalytic step at unattached kinetochores where immobilized heterodimers of Mad1-Mad2 act to catalyze a conformational change in inactive Mad2, producing an activated closed form (Kulukian et al., 2009). To this, our findings here have identified the mitotic checkpoint inhibitor to be produced by synergistic cooperation between Mad2 and BubR1. Mad2 binding reduces the affinity of the amino- and carboxy-terminal Cdc20 domains for each other, exposing a previously poorly accessible BubR1 binding site for Cdc20. This Mad2-dependent functional priming in Cdc20 is essential for BubR1's N terminus to produce the BubR1-Cdc20 mitotic checkpoint inhibitor (Figures 7C-7F;

(E and F) Time-lapse microscopy was used to determine the duration of mitosis in nocodazole (100 ng/ml)-treated cells after (1) depletion of endogenous (E) Mad2 (blue) or (F) BubR1 (blue), (2) replacement of endogenous Mad2 or BubR1 with (E) Mad2-AID-YFP (green) or (F) GFP-AID-BubR1 (green), and (3) induced destruction of (E) Mad2-AID-YFP (red) or (F) GFP-AID-BubR1 (red). Cells were treated with nocodazole prior to filming to facilitate accumulation of the mitotic checkpoint inhibitor(s). More than 60 cells were analyzed for each condition over three independent experiments. See also Figure S5.

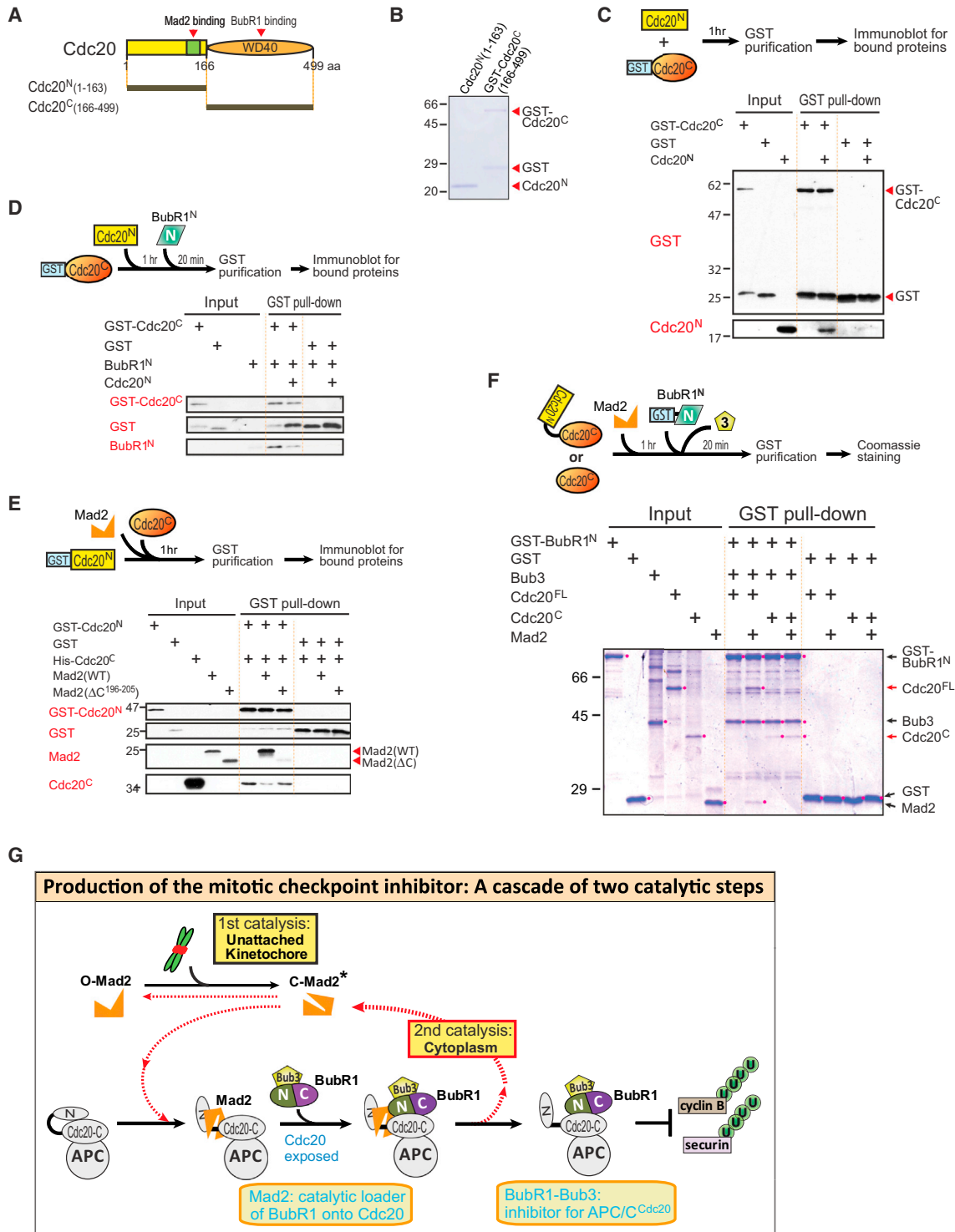


Figure 7. Mad2 Binding Unlocks Cdc20 to Allow Further Binding of BubR1

(A) Schematic of human Cdc20, showing the location of the N-terminal Mad2 binding domain and BubR1-binding WD40 repeat domain.

(B) Purified recombinant Cdc20 fragments assessed by Coomassie blue staining.

(C) GST-Cdc20^C or GST was affinity purified after incubation with Cdc20^N for 1 hr at room temperature. GST proteins and associated Cdc20^C were analyzed by immunoblotting.

(D) GST-Cdc20^C or GST was incubated with Cdc20^N for 1 hr and then further incubated with BubR1₁₋₃₆₃ for 20 min at room temperature before affinity purification. Associated proteins were analyzed by immunoblotting.

(legend continued on next page)

depleted of most Mad2 (our evidence), (3) continued inhibition of APC/C^{Cdc20} in mitotically arrested cells following in vivo targeted destruction of Mad2 (our evidence), and (4) the purification of a stable BubR1-Bub3-Cdc20 complex (free or APC/C bound) containing little Mad2 from cells under chronic mitotic checkpoint arrest (Kulukian et al., 2009; Nilsson et al., 2008). This model is also supported by prior work that has consistently shown Mad2 to have little ability to inhibit Cdc20 activation of APC/C at physiologically relevant concentrations (Fang, 2002; Kulukian et al., 2009; Sudakin et al., 2001).

Perhaps most importantly, we have shown that Mad2 released from the final inhibitory BubR1-Cdc20 complex can act catalytically to facilitate the loading of additional BubR1 molecules into inhibitory complexes with Cdc20 (Figure 6). We propose that this previously unappreciated catalytic step provides a means to cytosolically amplify initial kinetochore-derived Mad2-Cdc20 mitotic checkpoint complexes (Figure 7G), thereby allowing a single unattached kinetochore to globally inhibit APC/C^{Cdc20} activity. This model contrasts (in a crucial way) with a previous model that had proposed that cytosolic Cdc20-Mad2 complexes would amplify the number of Cdc20-Mad2 complexes, with each such complex acting in turn as an additional structural template to promote the conversion of additional open Mad2 molecules into a closed form that bound and inactivated Cdc20 (De Antoni et al., 2005). This latter model had been challenged (Doncic et al., 2005; Mariani et al., 2012), including on the grounds that, once initiated, the proposed amplification loop (amplifying the number of activated Mad2 molecules, just as the kinetochore does) would obligatorily continue independently of the kinetochore-derived signal and could not be silenced following attachment of the kinetochores to spindle microtubules. Our model, on the other hand, remains responsive to kinetochore-derived signaling and does not amplify the number of catalysts (i.e., activated, closed Mad2); instead, kinetochore-derived closed Mad2 is reused for two or more cycles, thereby providing an elevated number of APC/C^{Cdc20} inhibited by bound BubR1.

Finally, rather than being a stable component of the APC/C^{Cdc20} inhibitory complex, Mad2's continued association with APC/C^{Cdc20}-BubR1-Bub3 may instead contribute to the pathway of mitotic checkpoint silencing, where p31^{comet} has been proposed to facilitate dissociation of Mad2 and/or BubR1 from Cdc20 (Chao et al., 2012; Jia et al., 2011; Reddy et al., 2007; Teichner et al., 2011; Westhorpe et al., 2011) or destabilize Cdc20 bound to BubR1 and/or Mad2 (Varetti et al., 2011). Since our results have established that Mad2 dissociation from Cdc20 leaves a stable BubR1-Cdc20 interaction that continues to inhibit Cdc20 even after Mad2 release (Figures 3 and 4), our

evidence makes it highly unlikely that Mad2 extraction from the inhibitory Mad2-BubR1-Bub3-Cdc20 complex by p31^{comet} is a key step for checkpoint silencing. Instead, it is BubR1 dissociation from Cdc20 that is critical to reactivate APC/C^{Cdc20} for cyclin B recognition. While many aspects of mitotic checkpoint inactivation and p31^{comet} activity remain unresolved, we note that release from APC/C^{Cdc20} inhibition could be achieved by stimulating deacetylation-derived BubR1 degradation (Choi et al., 2009) or action of some checkpoint protein(s) (including p31^{comet}) stimulating Cdc20 degradation (Nilsson et al., 2008; Varetti et al., 2011), thereby facilitating the generation of active APC/C upon binding of newly synthesized Cdc20.

EXPERIMENTAL PROCEDURES

Constructs

Full-length and fragments of the human BubR1 open reading frame were cloned into either a pcDNA5/FRT/TO-based vector (Invitrogen) modified to contain an amino-terminal Myc-LAP epitope tag for mammalian cell expression or a pFastBac1-based vector (Invitrogen) modified to contain an amino-terminal GST-HRV 3C site for insect cell expression. The LAP tag consists of GFP-HRV 3C-6xHis BubR1^{HRV}, and Mad2^{HRV} mutants were generated using PCR-based site-directed mutagenesis to insert a HRV 3C site (LEVLFGQP) (QuikChange, Stratagene). For tetracycline-inducible expression of GFP-AID-BubR1 and Mad2-AID-YFP, the corresponding genes were cloned into a pcDNA5/FRT/TO-based vector (Invitrogen). All other DNA constructs were previously described (Kulukian et al., 2009; Tang et al., 2001).

Generation of Stable Cell Lines and siRNA Treatment

Parental Flp-In T-REX-HeLa parental cells that stably express monomeric red fluorescent protein (mRFP)-tagged histone H2B (H2B-mRFP) were as previously described (Gassmann et al., 2010). Stable, isogenic cell lines expressing MycGFP-BubR1 were generated using FRT/Flp-mediated recombination (Tighe et al., 2004). Expression of MycGFP-BubR1 was induced with 1 μg/ml tetracycline. siRNA directed against the 3' untranslated region of BubR1 (5'-CUGUAGUGUCUGUAAUUUA-3'; Figures 1 and 6) or GAPDH (5'-UGGUU UACAUGAUCC-AAUA-3') was purchased from Thermo Fisher Scientific. Cells were transfected with 50 nM of oligonucleotides using Lipofectamine RNAiMAX (Invitrogen). At 14 hr after transfection, tetracycline was added to express MycGFP-BubR1 for 24 hr before collecting cells for immunoblotting or analyzing by time-lapse microscopy. For IAA-inducible protein destruction, TIR1-TIR9Myc was introduced into Flp-In T-REX-DLD-1 parental cells (a kind gift from Stephen Taylor) using retroviral delivery (Shah et al., 2004). Stable integrates were selected in 2 μg/ml puromycin, and single clones were isolated using single-cell sorting (FACS Vantage; Becton Dickinson). Stable, isogenic cell lines expressing Mad2-AID-YFP or GFP-AID-BubR1 were generated using the FRT/Flp-mediated recombination and transgenes induced with tetracycline. To induce protein destruction, cells were treated with 500 μM of IAA. siRNA directed against the 3' untranslated region of BubR1 (5'-CUAACAGAC UCAUUUACAA-3'; Figure 5), Mad2 (5'-GGAAGAGUCGGGACCCAG-3'; Figures 1, 5, and 6), or p31^{comet} (5'-AGTGGTATGA GAAGTCCGAAG-3'; Figures 5 and 6) was used to deplete endogenous protein.

(E) GST-Cdc20^N or GST was incubated with Cdc20^C for 1 hr at room temperature in the presence of Mad2^{WT} or Mad2^{ΔC}. Associated Mad2 or Cdc20^C was analyzed by immunoblotting.

(F) GST-BubR1^N or GST was affinity purified after incubation with Cdc20^{FL} or Cdc20^C that had been preincubated with Mad2 or buffer and analyzed for associated Cdc20 and Mad2 by immunoblotting.

(G) Model for the production of the mitotic checkpoint through a cascade of two catalytic steps. Kinetochore generate a conformation change in Mad2, converting it from an open (O-Mad2) to a closed (C-Mad2) form. Binding of C-Mad2 to Cdc20 exposes Cdc20 for binding to BubR1 (first catalytic step). BubR1, but not Mad2, functions as an inhibitor for APC/C^{Cdc20}. Following loading of BubR1 onto Cdc20, Mad2 dissociates in a partially active closed conformation (C-Mad2*), which then either binds another free Cdc20 molecule to produce the BubR1-Cdc20 inhibitor (second catalytic step) or converts back to O-Mad2 and is used again in kinetochore signaling (first catalytic step). Thus, one Mad2 molecule produces multiple BubR1-Cdc20 inhibitors through two interlocking catalytic steps.

Live-Cell Microscopy

To determine mitotic timing, cells were seeded onto poly-L-lysine-coated coverglass chamber slides (Thermo Scientific) or poly-L-lysine-coated 35 mm glass-bottomed tissue culture dishes (MatTek) and transferred to supplemented CO₂-independent media (Invitrogen) 38–48 hr posttransfection. Cells were maintained at 37°C in an environmental control station, and images were collected using a DeltaVision RT System (Applied Precision) with a 40× 1.35 numerical aperture (NA) oil lens at 5 min time intervals. For each time point, 6 × 3 μM z sections were acquired for RFP, and maximum intensity projection was created using softWoRx. Movies were assembled and analyzed using QuickTime (Apple) or ImageJ software.

Protein Purification

GST- or His-tagged human BubR1, Bub3, and Cdc20 were expressed in Sf9 and High Five insect cells using the Bac-to-Bac expression system (Invitrogen) and affinity purified over nickel-nitrilotriacetic acid beads (QIAGEN) or glutathione sepharose beads (GE Healthcare). His-Mad2_{1–102} and other GST-tagged proteins were expressed from Rosetta *E.coli* after induction with IPTG and then purified (Kulukian et al., 2009). APC/C was immunoprecipitated from interphase *Xenopus* egg extracts as previously described (Kulukian et al., 2009).

APC/C Ubiquitination Activity Assay

The APC/C ubiquitination activity assay was performed as previously described (Tang and Yu, 2004), and activity was assessed by ubiquitination-derived depletion of cyclin B_{1–102} substrate (Tugendreich et al., 1995). Quantitative analysis of cyclin B_{1–102} depletion was performed as previously described (Kulukian et al., 2009). Briefly, the level of cyclin B_{1–102} was determined against a series of dilutions of the proteins.

APC/C Binding Assay

APC/C was immunoprecipitated from *Xenopus* interphase egg extracts for 2 hr at 4°C using a peptide-derived anti-Cdc27 antibody crosslinked to Affi-Prep protein A (Bio-Rad) beads. The APC/C beads were washed with Tris-buffered saline (TBS) supplemented with 0.4 M KCl and 0.1% Triton X-100 and incubated with Cdc20 and checkpoint proteins sequentially or simultaneously for the indicated time at room temperature. Unbound proteins were removed by washing the beads twice with 20 volumes of TBS buffer. APC/C complex was eluted from the beads by Cdc27 peptide competition as described (Herzog and Peters, 2005) and analyzed by immunoblotting.

In Vitro Binding Assay

In vitro binding assays were conducted in 50 mM Tris-HCl (pH 7.7), 100 mM KCl, 0.1% Triton X-100, 10% glycerol, and 1 mM DTT. Glutathione Sepharose-bound glutathione S-transferase (GST)-tagged protein and other recombinant proteins were combined and incubated at room temperature for 1 hr. Bound protein complexes were washed four times with 20 volumes of the binding buffer, eluted from the beads in 15 mM glutathione buffer, and analyzed by immunoblotting.

Antibodies

The antibodies used in this study are as follows: BubR1 (SBR1.1, a gift from S. Taylor; A300-386, Bethyl Laboratories), Bub3 (SB3.2, a gift from S. Taylor), Mad1 (BB3-8, a gift from A. Musacchio), Mad2 (A300-300A, Bethyl Laboratories), Cdc20 (A301-180A, Bethyl Laboratories), p31^{comet} (SC-134381, Santa Cruz Biotechnology), Myc (16-213, Millipore), Cdc27 (Herzog and Peters, 2005), α-tubulin (DM1α, Sigma-Aldrich), His (A00186, GenScript), and GST (SC-33613, Santa Cruz Biotechnology).

SUPPLEMENTAL INFORMATION

Supplemental Information includes five figures and can be found with this article online at <http://dx.doi.org/10.1016/j.molcel.2013.05.019>.

ACKNOWLEDGMENTS

We thank Stephen Taylor and Arshad Desai for providing reagents; Jennifer Meerloo of the University of California at San Diego Neuroscience Microscopy Shared Facility (NINDS P30 NS047101) for help with live-cell imaging; and Weijie Lan for help with preparation for *Xenopus* egg extracts. This work was supported by grant GM20513 from the NIH to D.W.C. Salary for J.S.H and A.J.H was supported in part by a senior fellowship from the Leukemia and Lymphoma Society. Salary support for D.W.C is provided by the Ludwig Institute for Cancer Research.

Received: January 27, 2012

Revised: November 9, 2012

Accepted: May 16, 2013

Published: June 20, 2013

REFERENCES

- Burton, J.L., and Solomon, M.J. (2007). Mad3p, a pseudosubstrate inhibitor of APC/Cdc20 in the spindle assembly checkpoint. *Genes Dev.* 21, 655–667.
- Chao, W.C., Kulkarni, K., Zhang, Z., Kong, E.H., and Barford, D. (2012). Structure of the mitotic checkpoint complex. *Nature* 484, 208–213.
- Choi, E., Choe, H., Min, J., Choi, J.Y., Kim, J., and Lee, H. (2009). BubR1 acetylation at prometaphase is required for modulating APC/C activity and timing of mitosis. *EMBO J.* 28, 2077–2089.
- Cordingley, M.G., Callahan, P.L., Sardana, V.V., Garsky, V.M., and Colonno, R.J. (1990). Substrate requirements of human rhinovirus 3C protease for peptide cleavage in vitro. *J. Biol. Chem.* 265, 9062–9065.
- Davenport, J., Harris, L.D., and Goorha, R. (2006). Spindle checkpoint function requires Mad2-dependent Cdc20 binding to the Mad3 homology domain of BubR1. *Exp. Cell Res.* 312, 1831–1842.
- De Antoni, A., Pearson, C.G., Cimini, D., Canman, J.C., Sala, V., Nezi, L., Mapelli, M., Sironi, L., Faretta, M., Salmon, E.D., and Musacchio, A. (2005). The Mad1/Mad2 complex as a template for Mad2 activation in the spindle assembly checkpoint. *Curr. Biol.* 15, 214–225.
- Doncic, A., Ben-Jacob, E., and Barkai, N. (2005). Evaluating putative mechanisms of the mitotic spindle checkpoint. *Proc. Natl. Acad. Sci. USA* 102, 6332–6337.
- Fang, G. (2002). Checkpoint protein BubR1 acts synergistically with Mad2 to inhibit anaphase-promoting complex. *Mol. Biol. Cell* 13, 755–766.
- Fang, G., Yu, H., and Kirschner, M.W. (1998). The checkpoint protein MAD2 and the mitotic regulator CDC20 form a ternary complex with the anaphase-promoting complex to control anaphase initiation. *Genes Dev.* 12, 1871–1883.
- Gassmann, R., Holland, A.J., Varma, D., Wan, X., Civril, F., Cleveland, D.W., Oegema, K., Salmon, E.D., and Desai, A. (2010). Removal of Spindly from microtubule-attached kinetochores controls spindle checkpoint silencing in human cells. *Genes Dev.* 24, 957–971.
- Herzog, F., and Peters, J.M. (2005). Large-scale purification of the vertebrate anaphase-promoting complex/cyclosome. *Methods Enzymol.* 398, 175–195.
- Holland, A.J., Fachinetti, D., Han, J.S., and Cleveland, D.W. (2012). Inducible, reversible system for the rapid and complete degradation of proteins in mammalian cells. *Proc. Natl. Acad. Sci. USA* 109, E3350–E3357.
- Hoyt, M.A., Totis, L., and Roberts, B.T. (1991). *S. cerevisiae* genes required for cell cycle arrest in response to loss of microtubule function. *Cell* 66, 507–517.
- Izawa, D., and Pines, J. (2012). Mad2 and the APC/C compete for the same site on Cdc20 to ensure proper chromosome segregation. *J. Cell Biol.* 199, 27–37.
- Jia, L., Li, B., Warrington, R.T., Hao, X., Wang, S., and Yu, H. (2011). Defining pathways of spindle checkpoint silencing: functional redundancy between Cdc20 ubiquitination and p31(comet). *Mol. Biol. Cell* 22, 4227–4235.
- King, E.M., van der Sar, S.J., and Hardwick, K.G. (2007). Mad3 KEN boxes mediate both Cdc20 and Mad3 turnover, and are critical for the spindle checkpoint. *PLoS ONE* 2, e342.

- Kulukian, A., Han, J.S., and Cleveland, D.W. (2009). Unattached kinetochores catalyze production of an anaphase inhibitor that requires a Mad2 template to prime Cdc20 for BubR1 binding. *Dev. Cell* 16, 105–117.
- Lara-Gonzalez, P., Scott, M.I., Diez, M., Sen, O., and Taylor, S.S. (2011). BubR1 blocks substrate recruitment to the APC/C in a KEN-box-dependent manner. *J. Cell Sci.* 124, 4332–4345.
- Lara-Gonzalez, P., Westhorpe, F.G., and Taylor, S.S. (2012). The spindle assembly checkpoint. *Curr. Biol.* 22, R966–R980.
- Lau, D.T., and Murray, A.W. (2012). Mad2 and Mad3 cooperate to arrest budding yeast in mitosis. *Curr. Biol.* 22, 180–190. Published online December 29, 2011. <http://dx.doi.org/10.1016/j.cub.2011.12.029>.
- Li, R., and Murray, A.W. (1991). Feedback control of mitosis in budding yeast. *Cell* 66, 519–531.
- Luo, X., Fang, G., Coldiron, M., Lin, Y., Yu, H., Kirschner, M.W., and Wagner, G. (2000). Structure of the Mad2 spindle assembly checkpoint protein and its interaction with Cdc20. *Nat. Struct. Biol.* 7, 224–229.
- Luo, X., Tang, Z., Rizo, J., and Yu, H. (2002). The Mad2 spindle checkpoint protein undergoes similar major conformational changes upon binding to either Mad1 or Cdc20. *Mol. Cell* 9, 59–71.
- Luo, X., Tang, Z., Xia, G., Wassmann, K., Matsumoto, T., Rizo, J., and Yu, H. (2004). The Mad2 spindle checkpoint protein has two distinct natively folded states. *Nat. Struct. Mol. Biol.* 11, 338–345.
- Mapelli, M., Filipp, F.V., Rancati, G., Massimiliano, L., Nezi, L., Stier, G., Hagan, R.S., Confalonieri, S., Piatti, S., Sattler, M., and Musacchio, A. (2006). Determinants of conformational dimerization of Mad2 and its inhibition by p31comet. *EMBO J.* 25, 1273–1284.
- Mapelli, M., Massimiliano, L., Santaguida, S., and Musacchio, A. (2007). The Mad2 conformational dimer: structure and implications for the spindle assembly checkpoint. *Cell* 131, 730–743.
- Mariani, L., Chirolì, E., Nezi, L., Müller, H., Piatti, S., Musacchio, A., and Ciliberto, A. (2012). Role of the Mad2 dimerization interface in the spindle assembly checkpoint independent of kinetochores. *Curr. Biol.* 22, 1900–1908.
- Nezi, L., Rancati, G., De Antoni, A., Pasqualato, S., Piatti, S., and Musacchio, A. (2006). Accumulation of Mad2-Cdc20 complex during spindle checkpoint activation requires binding of open and closed conformers of Mad2 in *Saccharomyces cerevisiae*. *J. Cell Biol.* 174, 39–51.
- Nilsson, J., Yekezare, M., Minshull, J., and Pines, J. (2008). The APC/C maintains the spindle assembly checkpoint by targeting Cdc20 for destruction. *Nat. Cell Biol.* 10, 1411–1420.
- Nishimura, K., Fukagawa, T., Takisawa, H., Kakimoto, T., and Kanemaki, M. (2009). An auxin-based degron system for the rapid depletion of proteins in nonplant cells. *Nat. Methods* 6, 917–922.
- Pan, J., and Chen, R.H. (2004). Spindle checkpoint regulates Cdc20p stability in *Saccharomyces cerevisiae*. *Genes Dev.* 18, 1439–1451.
- Peters, J.M. (2006). The anaphase promoting complex/cyclosome: a machine designed to destroy. *Nat. Rev. Mol. Cell Biol.* 7, 644–656.
- Reddy, S.K., Rape, M., Margansky, W.A., and Kirschner, M.W. (2007). Ubiquitination by the anaphase-promoting complex drives spindle checkpoint inactivation. *Nature* 446, 921–925.
- Shah, J.V., Botvinick, E., Bonday, Z., Furnari, F., Berns, M., and Cleveland, D.W. (2004). Dynamics of centromere and kinetochore proteins; implications for checkpoint signaling and silencing. *Curr. Biol.* 14, 942–952.
- Sironi, L., Melixetian, M., Faretta, M., Prosperini, E., Helin, K., and Musacchio, A. (2001). Mad2 binding to Mad1 and Cdc20, rather than oligomerization, is required for the spindle checkpoint. *EMBO J.* 20, 6371–6382.
- Sironi, L., Mapelli, M., Knapp, S., De Antoni, A., Jeang, K.T., and Musacchio, A. (2002). Crystal structure of the tetrameric Mad1-Mad2 core complex: implications of a 'safety belt' binding mechanism for the spindle checkpoint. *EMBO J.* 21, 2496–2506.
- Sudakin, V., Chan, G.K., and Yen, T.J. (2001). Checkpoint inhibition of the APC/C in HeLa cells is mediated by a complex of BUBR1, BUB3, CDC20, and MAD2. *J. Cell Biol.* 154, 925–936.
- Tang, Z., and Yu, H. (2004). Functional analysis of the spindle-checkpoint proteins using an in vitro ubiquitination assay. *Methods Mol. Biol.* 281, 227–242.
- Tang, Z., Bharadwaj, R., Li, B., and Yu, H. (2001). Mad2-independent inhibition of APC^{Cdc20} by the mitotic checkpoint protein BubR1. *Dev. Cell* 1, 227–237.
- Teichner, A., Eytan, E., Sitry-Shevah, D., Miniowitz-Shemtov, S., Dumin, E., Gromis, J., and Hershko, A. (2011). p31comet Promotes disassembly of the mitotic checkpoint complex in an ATP-dependent process. *Proc. Natl. Acad. Sci. USA* 108, 3187–3192.
- Tighe, A., Johnson, V.L., and Taylor, S.S. (2004). Truncating APC mutations have dominant effects on proliferation, spindle checkpoint control, survival and chromosome stability. *J. Cell Sci.* 117, 6339–6353.
- Tipton, A.R., Wang, K., Link, L., Bellizzi, J.J., Huang, H., Yen, T., and Liu, S.T. (2011). BUBR1 and closed MAD2 (C-MAD2) interact directly to assemble a functional mitotic checkpoint complex. *J. Biol. Chem.* 286, 21173–21179.
- Tugendreich, S., Tomkiel, J., Earnshaw, W., and Hieter, P. (1995). CDC27Hs colocalizes with CDC16Hs to the centrosome and mitotic spindle and is essential for the metaphase to anaphase transition. *Cell* 81, 261–268.
- Varetti, G., Guida, C., Santaguida, S., Chirolì, E., and Musacchio, A. (2011). Homeostatic control of mitotic arrest. *Mol. Cell* 44, 710–720.
- Vink, M., Simonetta, M., Transidico, P., Ferrari, K., Mapelli, M., De Antoni, A., Massimiliano, L., Ciliberto, A., Faretta, M., Salmon, E.D., and Musacchio, A. (2006). In vitro FRAP identifies the minimal requirements for Mad2 kinetochore dynamics. *Curr. Biol.* 16, 755–766.
- Weiss, E., and Winey, M. (1996). The *Saccharomyces cerevisiae* spindle pole body duplication gene MPS1 is part of a mitotic checkpoint. *J. Cell Biol.* 132, 111–123.
- Westhorpe, F.G., Tighe, A., Lara-Gonzalez, P., and Taylor, S.S. (2011). p31comet-mediated extraction of Mad2 from the MCC promotes efficient mitotic exit. *J. Cell Sci.* 124, 3905–3916.
- Wu, H., Lan, Z., Li, W., Wu, S., Weinstein, J., Sakamoto, K.M., and Dai, W. (2000). p55CDC/hCDC20 is associated with BUBR1 and may be a downstream target of the spindle checkpoint kinase. *Oncogene* 19, 4557–4562.
- Yang, M., Li, B., Tomchick, D.R., Machius, M., Rizo, J., Yu, H., and Luo, X. (2007). p31comet blocks Mad2 activation through structural mimicry. *Cell* 131, 744–755.
- Yang, M., Li, B., Liu, C.J., Tomchick, D.R., Machius, M., Rizo, J., Yu, H., and Luo, X. (2008). Insights into mad2 regulation in the spindle checkpoint revealed by the crystal structure of the symmetric mad2 dimer. *PLoS Biol.* 6, e50.